neuroimaging. I laid out the critical prediction derived from load theory, namely that visual cortex responses to distractor stimuli should depend on the level of load in the attended task, in the same manner as I had shown in my behavioural studies. About a year later, following a departmental seminar, Chris introduced me to his PhD student saying: "Geraint, this is Nilli: we will be testing together the critical prediction from her load theory". We then met in my office and quickly designed the study leading to our Rees, Frith and Lavie (1997) *Science* paper.

What are you up to these days?
Much of my work is still linked by a central focus on the effects of information load on brain mechanisms, various psychological functions (perception, conscious awareness, memory and emotion) and behavior. This central focus on load goes back to my PhD work, but while earlier on I focused on establishing the basic science behind these effects, I am now pursuing also some of the theory's applications for clinical populations and to everyday life.

For example, under some circumstances a high information load can lead to failures to notice important information (a phenomenon termed 'inattentional blindness'). This has a variety of practical implications, such as for better design of vehicles and aeroplanes: I am now collaborating with the automotive industry, pursuing applications of this to driving.

The effects of load on information processing can sometimes be positive as well. My research has shown that people are better able to ignore distracting stimuli when they perform a task that involves higher information load. This work suggests new ways of improving focused attention abilities, with implications that range from optimizing learning (for example, in educational settings), to helping individuals with attention difficulties (such as those with attention deficit hyperactivity disorder, 'ADHD') as currently pursued in my lab.

UCL Institute of Cognitive Neuroscience, 17 Queen Square, London WC1N 3AR, UK.
E-mail: n.lavie@ucl.ac.uk

Correspondence

Paget disease of bone in a Jurassic dinosaur

Florian Witzmann[1,*], Kerin M. Claeson[1,2,3], Oliver Hampe[1], Frank Wieder[3], André Hilger[3], Ingo Manke[3], Manuel Niederhagen[4], Bruce M. Rothschild[5], and Patrick Asbach[6]

Paget disease of bone — initially described by Sir James Paget in 1876 — is a benign bone disorder well known in human pathology. It leads to the enlargement and deformity of bones due to a combination of abnormal bone resorption and abundant new bone formation [1–3]. There is strong evidence that viruses are involved in the disease, coupled with a probable genetic component [3,4]. Paget disease in humans most frequently involves the skull, the spine and parts of the pelvis [1–3]. There is only limited evidence on Paget disease in other extant mammals, such as orangutans and lemurs [5]. Paget disease has also been described in human bones dating back to the Neolithic [6]. Here, we report Paget disease in a vertebra of the Jurassic dinosaur *Dysalotosaurus lettowvorbecki*, representing the oldest indirect evidence of viruses in the fossil record.

The diagnosis of Paget disease in humans is based on features observed through radiologic examination and laboratory testing [1–3,7]. Characteristic radiologic features allow accurate diagnosis comprising the classical triad of thickening of the cortex, coarsening of the trabecular pattern and increased size of the bone [1]. In some less conclusive cases, nuclear medicine may aid in diagnosis through demonstrating increased isotope activity in the affected bone due to high bone turnover [1].

Paget disease can occur in three phases — osteolytic, mixed and blastic [1,2]. In the initial osteolytic phase, bone resorption and replacement of hematopoietic bone marrow

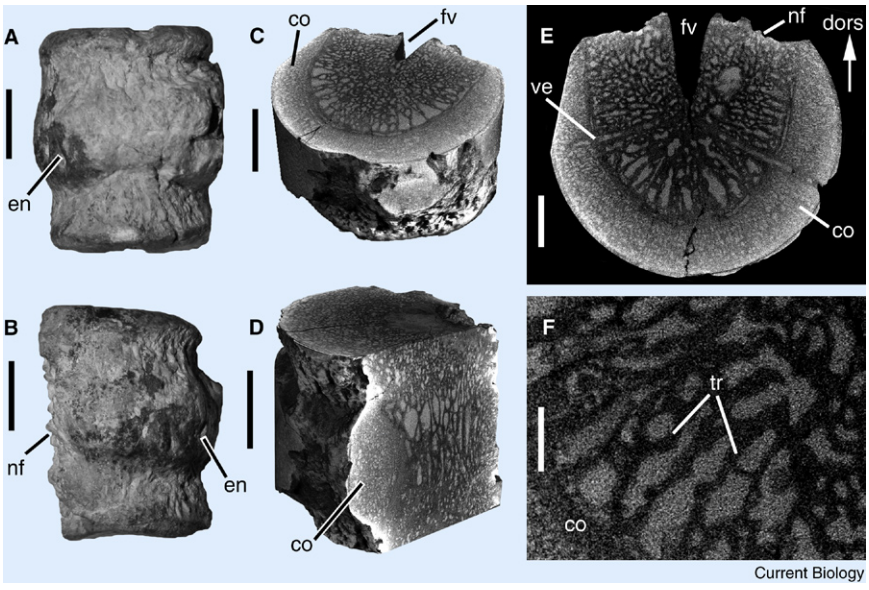

Figure 1. Paget disease in a dinosaur.
Pathologic vertebra of the dinosaur *Dysalotosaurus lettowvorbecki* (MB.R.1336) from the Upper Jurassic of Tanzania. (A) Photograph of the vertebral body in ventral view; scale bar equals 10 mm. (B) Photograph of the vertebral body in lateral view, dorsal is to the left; scale bar equals 10 mm. (C) Three-dimensional micro-CT image with transverse cross-section through enlarged middle part of the bone, dorsal is top right; scale bar equals 10 mm. (D) Three-dimensional micro-CT image with transverse cross section in the region of one endplate and sagittal section; scale bar equals 10 mm. (E) Transverse cross-section micro-CT image through enlarged middle part of the bone; the trabecular pattern of the vertebra is well preserved, thickening of the cortex contributes to bone enlargement, and small calibre vessels course through the dense cortex; scale bar equals 5 mm. (F) Transverse cross-section micro-CT image through enlarged middle part of the bone showing trabecular morphology; scale bar equals 1 mm (Supplemental information). Abbreviations: co = cortex; dors = dorsal; en = enlargement in middle part of bone; fv = foramen venosum; nf = neurocentral sutural facet; tr = trabecula; ve = vessel.

by fibrous connective tissue are present, identifiable as lytic lesions on radiographs. In the mixed phase, which is present in the vast majority of human cases, lytic and blastic changes coexist, resulting in a pattern of trabecular coarsening and thickening, as well as cortical thickening. Affected vertebral bodies at the mixed phase may show a 'picture-frame' appearance on radiographs, caused by the thickening of the dense cortex [2]. During the final blastic or sclerotic phase, abnormal bone enlargement and hardening are particularly common. When an entire vertebral body undergoes sclerotic alteration during the blastic phase, it takes on an 'ivory-vertebra' appearance on radiographs [2].

We studied a vertebral body of the bipedal, small ornithopod dinosaur *Dysalotosaurus lettowvorbecki* from the Late Jurassic (150 million years ago) of the Tendaguru locality in Tanzania (Supplemental information). This specimen is stored in the Museum für Naturkunde in Berlin (inventory number MB.R.1336). Macroscopically, the vertebral body shows near-uniform enlargement in the middle part of the bone with an irregular brassicate surface texture (Figure 1A,B). Micro-CT scans of the specimen demonstrate the characteristic radiologic imaging triad of Paget disease during the mixed phase (Supplemental information). These include a coarsening of the trabecular bone most prominent in the central and inferior portion of the vertebral body (Figure 1C-F), with thickening of the trabeculae in an anteroposterior direction. Enlargement is well delineated on the sagittal and coronal sections (Figure 1D; Supplemental information). In addition, the quantification of trabecular bone volume by means of segmentation demonstrated an increase from 34.7% (±1.0%) in a healthy control specimen (normal vertebral body of the same species, MB.R.1586) to 74.8% (±2.2%) in the pathologic specimen (Supplemental information). This is comparable to the more than two-fold increase that was found in a recent human study applying quantitative histomorphometry [7]. The cortex is also thickened as a result of high bone turnover and the vertebral body is consequently enlarged. The thickened cortex involves one endplate and the ventral and lateral margin. The opposite endplate and the dorsal margin are not involved (Supplemental information). Small calibre vessels coursing through the dense cortex are also observed. An increase in cell number is evident (Supplemental information) and correlated with the increase in cell number previously described in humans [7].

Evidence of Paget disease of bone in the fossil record is of particular significance for several reasons. First, viral infection is thought to be a major component of the etiology of Paget disease [3,4]. Second, there is a genetic component of Paget disease reflected by the presence of familial and sporadic forms of Paget [3]. There is evidence that mutations in the *SQSTM1* gene are present in ~40–50% of familial Paget disease cases and in 5–10% of cases of the sporadic form [3]. Results from epidemiologic studies suggest that *SQSTM1* is likely a disease susceptiblity gene rather than a disease-causing gene, where mutations are triggered by exposure to a disease-associated environmental factor [4,7]. There is strong evidence that those environmental factors include viruses (e.g. measles) [4]. In particular, there are nuclear inclusion bodies resembling paramyxoviruses found in osteoclast nuclei affected by Paget disease [8]. Thus, at present, Paget disease of bone can be considered as indirect evidence of the presence of viruses.

Potential direct evidence of viruses in fossil insects in Early Cretaceous amber was previously reported [9]. There is, however, scepticism as to whether the proposed findings are nonspecific microcrystals rather than viral constituents [10]. Our findings based on the analysis of the *Dysalotosaurus* vertebra suggest that Paget disease of bone evolved at least 150 million years ago and probably affected dinosaurs in a similar fashion as it does humans given identical radiologic imaging findings. Considering the viral component to Paget disease, our results indicate that paramyxovirus-like pathogens also would have evolved at least 150 million years ago. The case of Paget disease of bone presented here is, thus, substantially older than any previously reported [6]. Our results add palaeopathologic evidence to the commonly regarded fact that most common disease etiologies, such as traumatic, neoplastic, autoimmune, developmental, toxic/metabolic and infectious/inflammatory, were present and evolving for millions of years and crossed several species barriers [5].

Supplemental Information

Supplemental Information includes supplemental results, discussion and experimental procedures and can be found with this article online at doi:10.1016/j.cub.2011.08.006.

Acknowledgements

We would like to thank A. Paulke and N. Kardjilov (Helmholz Centre Berlin) for their support during experiments and image analysis, and D. Schwarz-Wings (Museum für Naturkunde Berlin) for access to the collection under her care and the loan of specimens. The authors declare no conflict of interests.

References

1. Smith, S.E., Murphey, M.D., Motamedi, K., Mulligan, M.E., Resnik, C.S., and Gannon, F.H. (2002). From the archives of the AFIP. Radiologic spectrum of Paget disease of bone and its complications with pathologic correlation. Radiographics *22*, 1191–1216.
2. Dell'Atti, C., Cassar-Pullicino, V.N., Lalam, R.K., Tins, B.J., and Tyrrell, P.N.M. (2007). The spine in Paget's disease. Skeletal Radiol. *36*, 609–626.
3. Roodman, G.D., and Windle, J.J. (2005). Paget disease of bone. J. Clin. Invest. *115*, 200–208.
4. Reddy, S.V., Singer, F.R., and Roodman, G.D. (1995). Bone marrow mononuclear cells from patients with Paget's disease contain measles virus nucleocapsid messenger ribonucleic acid that has mutations in a specific region of the sequence. J. Clin. Endocrinol. Metab. *80*, 2108–2111.
5. Rothschild, B.M., and Martin, L.D. (2006). Skeletal impact of disease. Bull. New Mexico Mus. Natl. Hist. *33*, 1–226.
6. Roches, E., Blondiaux, J., Cotton, A., Chastanet, P., and Flipo, R.M. (2002). Microscopic evidence for Paget's disease in two osteoarchaeological samples from early northern France. Int. J. Osteoarchaeol. *12*, 229–234.
7. Seitz, S., Priemel, M., Zustin, J., Beil, F.T., Semler, J., Minne, H., Schinke, T., and Amling, M. (2009). Paget's disease of bone: histologic analysis of 754 patients. J. Bone Miner. Res. *24*, 62–69.
8. Mills, B.G., and Singer, F.R. (1976). Nuclear inclusions in Paget's disease of bone. Science *194*, 201–202.
9. Poinar, G. Jr., and Poinar, R. (2005). Fossil evidence of insect pathogens. J. Invertebr. Pathol. *89*, 243–250.
10. Grimaldi, D. (2009). Did disease indeed destroy the dinosaurs? BioSience 59, 446–447.

[1]Leibniz Institute for Research on Evolution and Biodiversity at the Humboldt University Berlin, Museum für Naturkunde, Invalidenstraße 43, 10115 Berlin, Germany. [2]Department of Geological Sciences, The Jackson School of Geosciences, University of Texas at Austin, Austin, TX 78712-0294, USA. [3]Helmholtz Centre for Materials and Energy (HZB), Hahn-Meitner-Platz 1, 14109 Berlin, Germany. [4]Department of Pathology, Ludwig-Maximilians-Universität München, Marchioninistr. 27, 81377 Munich, Germany. [5]Biodiversity Center, University of Kansas, Lawrence, KS 66045, USA. [6]Department of Radiology, Charité - Universitätsmedizin Berlin, Charitéplatz 1, 10117 Berlin, Germany.
*E-mail: florian.witzmann@mfn-berlin.de

Supplemental information:

Paget disease of bone in a Jurassic dinosaur

Florian Witzmann, Kerin M. Claeson, Oliver Hampe, Frank Wieder, André Hilger,
Ingo Manke, Manuel Niederhagen, Bruce M. Rothschild, and Patrick Asbach

Supplemental Experimental Procedures

Microfocus X-ray computed tomography (mCT) was used to image the internal structure of the *Dysalotosaurus* vertebrae. The mCT scans were performed at the Helmholtz Centre Berlin for Materials and Energy (HZB), using a microfocus X-ray tube (Hamamatsu, L8121-03) at 100 kV tube voltage, 100 µA tube current, and a spotsize of 7 µm. A 1 mm aluminium window served as beam filter. Exposure time was set to 1 second per projection image. The detector was a 2316 x 2316 pixel Hamamatsu flat panel sensor (C7942SK-05).

The synchrotron X-ray phase contrast tomography investigations were carried out at the tomography station at the BAMline (electron storage ring Bessy, HZB, Germany) [S1]. A W-Si multilayer monochromator with an energy resolution of about $dE/E \sim 10^{-2}$ was used to obtain a monochromatic 30 keV X-ray beam. A CWO (cadmium tungstate) scintillator screen was used to convert X-rays into visible light that was detected by a 4008 x 2672 pixel CCD detector (PCO4000). The used pixel size was about 0.43 µm. 2700 radiographic projection images were recorded over 180°, i.e. images were recorded at intervals of 0.067°. Exposure time was 2 seconds per image. A distance of 220 mm between sample and detector was used for edge enhancement (phase contrast) to increase image contrast.

Axial cross sectional images were reconstructed with a slice thickness of about 12 µm (mCT) and 0.43 µm (synchrotron X-ray phase contrast tomography) using Octopus (Institute for Nuclear Sciences, Ghent, Belgium). Resulting thin sections were processed using the volume

rendering programme VG StudioMax version 1.2 (Volume Graphics, Heidelberg, Germany). For segmentation of the trabecular bone volumes a threshold between the attenuation coefficient of the trabecular bone and the surrounding material was applied (Software VGStudiomax).

Supplemental information on *Dysalotosaurus lettowvorbecki*

The specimen under study is a vertebral body of the bipedal, small-growing herbivorous ornithopod dinosaur *Dysalotosaurus lettowvorbecki* from the Late Jurassic (late Kimmeridgian; ca. 150 my ago) of the Tendaguru locality in Tanzania [S2]. This specimen is stored in the Museum für Naturkunde in Berlin under the inventory number MB.R.1336. This isolated vertebra was found between October 1910 and December 1912 during the German Tendaguru expedition in the largely monospecific bonebed “dy” [S3] and therefore cannot be associated with a specific individual. The neural arch, which was connected to the centrum by nonossified neurocentral sutures in the living animal, is not preserved. This indicates that the specimen was not fully grown. *Dysalotosaurus lettowvorbecki* is the smallest known dinosaur from the Tendaguru site and reached lengths between two and four meters. Thousands of skeletal remains of this species were discovered only at this locality, from isolated bones to partially preserved skeletons, giving strong evidence that these animals probably lived in herds [S4]. The length and shape of the hind limbs indicates *Dysalotosaurus* as a fast bipedal runner with cursorial adaptations [S5-S7]. Phylogenetic analyses show that *Dysalotosaurus* and its allies (*Dryosaurus*, *Valdosaurus*, ?*Planicoxa*) are closely related to *Iguanodon* and higher ornithopods [S8-S11].

Supplemental results and discussion

Trabecular pattern: Coronal cross sectional images were obtained from the abnormal vertebral body and a normal vertebral body of the same species (MB.R.1586) for comparison

using microfocus computed tomography. Thickening is well delineated on the coronal images (Supplemental Fig. 1A) as compared to a normal trabecular pattern (Supplemental Fig. 1B). Synchrotron X-ray phase contrast tomography images demonstrate the increase in trabecular number and coarsening of the trabecular pattern of the pathologic vertebral body compared to the normal specimen in detail, and show the increase in number of bone cells in the pathologic specimen (Supplemental Fig. 2).

Differential diagnoses: Differential diagnoses concerning the pathology in the *Dysalotosaurus* vertebra MB.R.1336 are rejected as follows. 1) Fracture with callus formation is rejected because there is no height loss or compression deformity present and the endplates are oriented in a parallel formation. In addition, the dense cortex of MB.R.1336 shows an organised internal structure, which is not seen in the case of fracture callus. Finally, the structure of the orientation of the trabecular pattern is homogeneous, i.e., there are no lines of collapsed trabeculae seen in a fracture line pattern [S12]. 2) A malignant solid bone neoplasm is rejected because MB.R.1336 lacks the typical onion-skin configuration of the outer margin (i.e., areas of lysis are absent) and the trabecular bone again is too homogeneous for neoplastic involvement with no mottled appearance [S12]. 3) A benign vascular neoplasm such as cavernous or epithelioid hemangioma is rejected because those kinds of lesions are associated with central lytic areas and a diffuse sclerosis of bone in peripheral areas [S12]. In addition, benign vascular neoplasms do not exhibit significant enlargement of the vertebral body. 4) Fibrous dysplasia is rejected because it is characterised by a ground glass appearance and expansive character of the areas of bone involved. The bone formation in fibrous dysplasia consists of irregular, immature bone trabeculae that are not associated with the local trabecular structure of the affected bone [S12]. Furthermore, fibrous dysplasia does not demonstrate new bone formation. 5) Chronic osteomyelitis is rejected because it would include an area of lysis and periosteal apposition would be heterogeneous, with no internal

structure [S12]. 6) Osteomalacia is rejected because it is characterised by rarefication of the entire vertebral body, in addition to trabecular structure, and would not show thickening of the cortex [S12]. The pathognomonic radiological appearance of the *Dysalotosaurus* vertebral body presented here is similar to the radiological appearance of Paget disease in humans (see main text). Therefore, after excluding the above-mentioned differential considerations, we attribute the morphologic and radiologic appearance of MB.R.1336 to Paget disease of bone.

Supplemental references

S1. Görner, W., Hentschel, M.P., Müller, B.R., Riesemeier, H., Krumrey, M., Ulm, G., Diete, W., Klein, U., and Frahm, R. (2001). BAMline: the first hard X-ray beamline at BESSY II. Nucl. Instrum. Meth. *A 467*, 703.

S2. Bussert, R., Heinrich, W.D., and Aberhan, M. (2009). The Tendaguru Formation (Late Jurassic to Early Cretaceous, southern Tanzania): definition, palaeoenvironments, and sequence stratigraphy. Foss. Rec. *12*, 141–174.

S3. Heinrich, W.D. (1999). The taphonomy of dinosaurs from the Upper Jurassic of Tendaguru (Tanzania) based on field sketches of the German Tendaguru Expedition (1909–1913). Mitt. Mus. Natkd. Berlin, Geowiss Reihe *2*, 25–61.

S4. Heinrich, W.D., Bussert, R., and Aberhan, M. (2011). A blast from the past: the lost world of dinosaurs at Tendaguru, East Africa. Geol Today *27*, 101–106.

S5. Janensch, W. (1955). Der Ornithopode *Dysalotosaurus* der Tendaguruschichten. Palaeontogr. Abt. A Suppl. *7*, 105–176.

S6. Galton, P.M. (1981). *Dryosaurus*, a hypsilophodontid dinosaur from the Upper Jurassic of North America and Africa: postcranial skeleton. Palaeontol. Z. *55*, 271–312.

S7. Galton, P.M. (1983). The cranial anatomy of *Dryosaurus*, a hypsilophodontid dinosaur from the Upper Jurassic of North America and East Africa, with review of the

hypsilophodontids from the Upper Jurassic of North America. Geol. Palaeontol. *17*, 207–243.

S8. Norman, D.B. (1990). A review of the Wealden iguanodontid dinosaur *Vectisaurus valdensis* Hulke 1874, with comments upon the status of the family Iguanodontidae. In Dinosaur systematics: approaches and perspectives, K. Carpenter and P.J. Currie, eds (Cambridge: Cambridge University Press), pp. 147–161.

S9. Norman, D.B. (1998). On Asian ornithopods (Dinosauria: Ornithischia). III. A new species of iguanodontid dinosaur. Zool. J. Linn. Soc. *122*, 291–348.

S10. Norman, D.B. (2004). Basal Iguanodontia. In The Dinosauria. Second edition, D.B. Weishampel, P. Dodson, and H. Osmolska, eds. (Berkeley: University of California Press), pp. 413–437.

S11. Coria, R.A., and Salgado, L. (1996). A basal iguanodontian (Ornithischia: Ornithopoda) from the Late Cretaceous of South America. J. Vert. Paleontol. *16*, 445–457.

S12. Greenspan, A., and Remagen, W. (1998). Differential Diagnosis of Tumors and Tumor-like Lesions of Bones and Joints (Philadelphia: Lippincott-Raven).

Supplemental figures

Supplemental Figure 1. Coronal cross section micro-CT images of *Dysalotosaurus lettowvorbecki* vertebrae. **(A)** The thickened cortex in the pathologic specimen MB.R.1336 involves one endplate and the ventral and lateral margin, coarsening and thickening of the trabecular pattern results in a disorganised configuration. **(B)** Normal vertebral body MB.R.1586 for comparison showing normal trabecular structure. Scale bar equals 10 mm.

Supplemental Figure 2. Cross sections of the synchrotron X-ray phase contrast tomogram. **(A)** Pathologic specimen MB.R.1336 demonstrating the increase in number of bone cells (arrows). **(B)** Normal specimen MB.R.1586 with lower number of cells for comparison. Scale bars equal 0.09 mm. Arrows point to bone cell lacunae (black dots). Abbreviation: tr = trabecula.

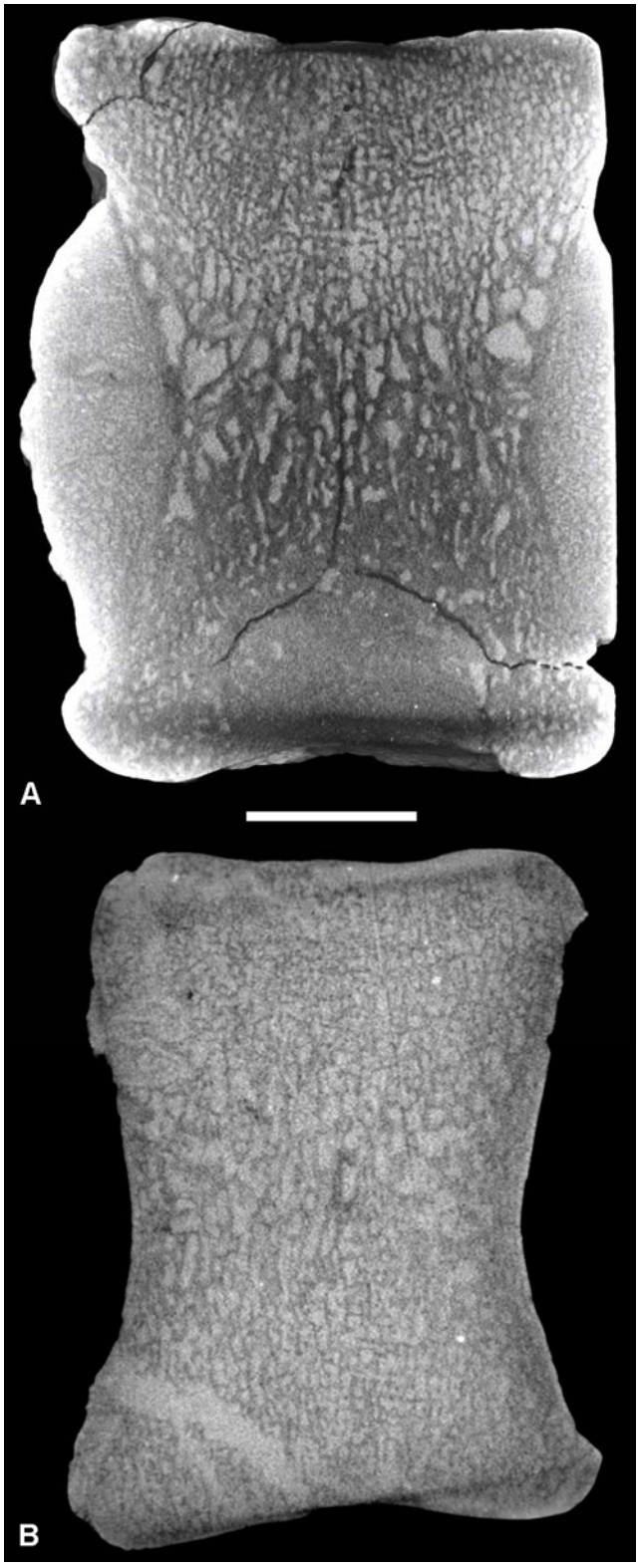

Supplemental Figure 1.

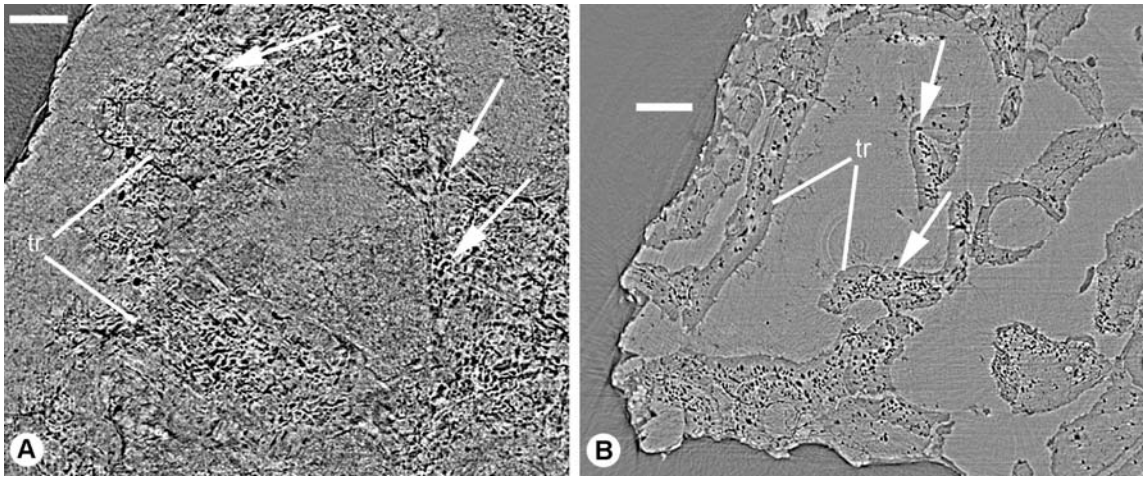

Supplemental Figure 2.